Draft version December 2, 2019
Preprint typeset using LaTeX style emulateapj v. 11/10/09

BREAKDOWN OF KENNICUTT-SCHMIDT LAW AT GMC SCALES IN M33

Sachiko Onodera[1,2], Nario Kuno[1,8], Tomoka Tosaki[1,3], Kotaro Kohno[2], Kouichiro Nakanishi[4,8], Tsuyoshi Sawada[4], Kazuyuki Muraoka[5], Shinya Komugi[6], Rie Miura[7], Hiroyuki Kaneko[8], Akihiko Hirota[1], and Ryohei Kawabe[1]

Draft version December 2, 2019

ABSTRACT

We have mapped the northern area ($30' \times 20'$) of a local group spiral galaxy M33 in ^{12}CO(J=1–0) emission line with the 45-m telescope at Nobeyama Radio Observatory (NRO). Along with the Hα and Spitzer 24 μm data, we have investigated the relationship between the surface density of molecular gas mass and the star formation rate (SFR) in an external galaxy (Kennicutt-Schmidt law) with the highest spatial resolution ($\sim$ 80 pc) to date. This resolution is comparable to the scale of giant molecular clouds (GMCs). At the positions where CO is detected, the SFR surface density exhibits a very wide range of up to four orders of magnitude, from $\Sigma_{\rm SFR} \lesssim 10^{-10}$ to $\sim 10^{-6}\ M_\odot\ {\rm yr}^{-1}\ {\rm pc}^{-2}$, whereas the $\Sigma_{\rm H_2}$ values are mostly in the range of 10–40 $M_\odot\ {\rm pc}^{-2}$. It is found that the gas surface density and SFR correlate well at a resolution of $\sim$1 kpc, but it becomes looser with higher resolution and breaks down at GMC scales. The scatter of the $\Sigma_{\rm SFR}$–$\Sigma_{\rm H_2}$ relationship in the $\sim$80 pc resolution results from the variety of star forming activity among GMCs. Their variety is attributed to the drift of young clusters from their parent GMCs and to the variety in the evolutionary stages of GMCs. This result shows that the Kennicutt-Schmidt law is valid only in scales larger than that of GMCs, when we average the spatial offset between GMCs and the star forming regions, and their various evolutionary stages.

1. INTRODUCTION

Understanding the formation process of massive stars in galaxies is one of the key issues in modern astronomy because massive stars play essential roles in the evolution of galaxies. Because stars are formed from molecular gas, the study of molecular gas in galaxies provides us with important clues to the fundamental physical processes of massive star formation in galaxies. Observational studies of galaxies on global scales have shown that the surface density of star formation rate (SFR) and that of cold gas obey a simple relation, $\Sigma_{\rm SFR} \propto \Sigma_{\rm gas}^n$, where $\Sigma_{\rm SFR}$ is the SFR per unit area and $\Sigma_{\rm gas}$ is the surface density of gas. This relationship is known as the Kennicutt-Schmidt law (hereafter, K-S law: Schmidt 1959; Kennicutt 1998). It has been shown that the disk-averaged surface density of SFR is much better correlated with the surface density of molecular gas $\Sigma_{\rm H_2}$ than with that of total (HI + $\rm H_2$) gas $\Sigma_{\rm HI+H_2}$ (e.g., Wong & Blitz 2002).

Because almost all of the existing observational studies on the K-S law in galaxies have been carried out based on CO observations of kpc-scale resolution or disk-averaged data (e.g., Komugi et al. 2005), not much is known about the validity of the K-S law for smaller molecular structures such as giant molecular associations (GMAs) and giant molecular clouds (GMCs). Recently, Kennicutt et al. (2007) investigated K-S law in M51 down to a linear scale of 500 pc and cloud mass scales of 10^6–$10^7\ M_\odot$. They found that the nonlinear the K-S law can be extended down to that scale. Verley et al. (2010) have shown that a loose correlation exists even in the 180 pc scale in M33. It is of interest to determine the smallest scale in which the K-S law can be applied.

Because most of the molecular gas is confined within molecular clouds and virtually all of the GMCs are sites of star formation in the Milky Way, GMCs play an important role in star formation. For example, Kawamura et al. (2009) studied the Large Magellanic Cloud and revealed the evolutionary processes of GMCs from young molecular clouds to those that are consumed and dissolved by newborn stars. It is important to understand how star formation at GMC scales is linked to the K-S law, which is valid for kpc-scales.

One of the means to address this issue is to conduct a high-spatial resolution mapping of entire molecular gas disks in the nearest galaxies. The recent improvements in the resolution, sensitivity, and observing efficiency of radio telescopes have made such observational studies feasible.

M33 is the best target for this purpose. It is one of the nearest spiral galaxies (D=840 kpc; Freedman et al. 1991) in which individual GMCs can be resolved with the present instruments. Furthermore, because its disk

sonodera@nro.nao.ac.jp
[1] Nobeyama Radio Observatory, National Astronomical Observatory, 462-2, Nobeyama, Minamimaki, Minamisaku, Nagano 384-1305, Japan
[2] Institute of Astronomy, The University of Tokyo, 2-21-1 Osawa, Mitaka, Tokyo 181-0015, Japan
[3] Joetsu University of Education, Yamayashiki-machi, Joetsu, Niigata 943-8512, Japan
[4] ALMA Project Office, National Astronomical Observatory, 2-21-1 Osawa, Mitaka, Tokyo 181-8588, Japan
[5] Osaka Prefecture University, 1-1 Gakuen-cho, Nakaku, Sakai, Osaka 599-8531, Japan
[6] Japan Aerospace Exploration Agency, Institute of Space and Astronautical Science 3-1-1 Yoshinodai, Sagamihara, Kanagawa 229-8510, Japan
[7] Department of Astronomy, Graduate School of Science, The University of Tokyo, 7-3-1 Hongo, Bunkyo-ku, Tokyo 113-0033, Japan
[8] The Graduate University for Advanced Studies (Sokendai), 2-21-1 Osawa, Mitaka, Tokyo 181-8588, Japan

is moderately face-on (i=51°), it is easy to study the molecular gas in relation to star formation.

Because of these desirable characteristics, M33 has been the subject of many large-scale studies of GMC. Pioneering surveys of the central 1.7 kpc region of M33 were conducted with the 12-m telescope of the of the National Radio Astronomy Observatory (Wilson & Scoville 1989) and the Owens Valley Radio Observatory interferometer (Wilson & Scoville 1990). They revealed that the properties of GMCs (velocity width, diameter, peak brightness temperature, and mass) were very similar to those in the Milky Way Galaxy. More recently, a CO (J=1–0) all-disk survey was performed with the Berkeley-Illinois-Maryland Association (BIMA) (Engargiola et al. 2003), which identified 148 GMCs with masses over $1.5\times10^5 M_\odot$ across the star-forming disk. The BIMA survey recovered only 20% of the CO flux in M33 because of the missing short spacings of the interferometer (Heyer et al. 2004); thus, Rosolowsky et al. (2007) performed additional CO (J=1–0) observations with the 45-m telescope of the Nobeyama Radio Observatory (NRO), and combined them with the existing data obtained from BIMA and 14-m telescope at the Five College Radio Astronomy Observatory (FCRAO). They obtained the CO (J=1–0) map in the inner $\sim15'\times15'$ ($\sim$3.7 kpc) region at a resolution of $20''$ ($\sim$80 pc).

However, these observations are still insufficient to understand the overall nature of the GMCs in M33 because they do not cover the entire disk, and has they possess inhomogeneities due to multi-field interferometric observations. Accordingly, a homogeneous wide-area single-dish mapping with a high spatial resolution and high sensitivity is required in order to determine the molecular gas properties of the entire disk.

In order to achieve this purpose, it is effective to adopt the on-the-fly (OTF) mapping technique using a single-dish telescope having a large aperture. We are performing an M33 all-disk ^{12}CO(J=1–0) survey with the 45-m telescope, as an NRO legacy project to study the properties and evolution of GMCs and star formation within the entire galaxy. In this paper, we investigate the K-S law in the GMC scale which is the highest resolution ($\sim$80 pc) to date, as an initial result of this project.

2. OBSERVATIONS AND DATA

We observed the ^{12}CO (J=1–0) emission lines toward the north in a $30'\times20'$ ($\sim$7.3 kpc $\times$ 4.9 kpc) region of M33; the observation region covered the galactic center and the three major HII regions: NGC 604, NGC 595, and IC 133. The mapping area is shown in Fig. 1.

The observations were carried out from January to April, 2008, with the 45-m telescope at NRO. The beam size of the telescope (HPBW) was $15''$ for the rest frequency of the ^{12}CO (J=1–0) emission line (115.271204 GHz). We used the 25-BEam Array Receiver System (BEARS: Sunada et al. 2000). Because BEARS is a double side band receiver, we measured the sideband ratios of each beam of BEARS by observing a bright standard source NGC 7538 with both BEARS and a single-beam receiver S100 equipped with a single side band filter. The errors in the scaling factors of BEARS were smaller than $\sim$20%. The main beam efficiency measured with S100 was $\eta_{\rm MB}=0.32\pm0.02$ at 115 GHz. The typical system temperature was $\sim$ 700 K (SSB). We used digital autocorrelators as backends. The spectrometers have 1024 channels covering a bandwidth of 512 MHz with a frequency resolution of 1.0 MHz, which corresponds to 1332 km s^{-1} and 2.6 km s^{-1}. The chopper-wheel technique was employed to calibrate the antenna temperature $T_{\rm A}^*$. Hereafter all the CO intensity measurements will be mentioned in the $T_{\rm MB}$ ($\equiv T_{\rm A}^*/\eta_{\rm MB}$) scale.

The observations were performed using the OTF observation mode (Sawada et al. 2008). Throughout the observations, the data were sampled every 0.1 s. The emission-free "OFF" points were taken at an offset of $30'$ from the center. We checked the pointing accuracy every hour with a 5-point observation of a SiO maser source IRC+30021 with a 43 GHz SIS receiver (S40). We excluded all the data in the observation sequence that had pointing errors larger than $7''.5$ or with wind speed greater than 10 m s^{-1} to avoid the systematic intensity loss due to pointing errors. After these data screenings, the net integration time was determined to be approximately 130 h.

The data reductions were made with the OTF reduction software package NOSTAR, which was implemented by the NRO. The data were convolved with a Gaussian-tapered Jinc function to create the spectral data cube. The grid spacing was taken as $7''.5$, and the spatial resolution of the final map was $19''.3$. Finally, the baselines were fitted and subtracted from the data cube. The velocity resolution of the final cube is 2.5 km s^{-1}. The rms noise in a velocity channel was 130 mK. The rms noise in the integrated intensity map was 1.6 K km s^{-1}, which corresponds to a mass sensitivity of 4.8 $M_\odot$ pc^{-2}.

3. RESULTS

3.1. *CO (J=1–0) map*

Fig. 1 shows the CO (J=1–0) integrated intensity map of our observation field for M33. It reveals the clumpy nature of the molecular gas distribution. The size of these clumps ranges from $\lesssim$ 100 pc (comparable to our beam size) to 500 pc, which corresponds to that of GMCs and/or GMAs. The northern arm that can be traced from (α, δ) = ($1^{\rm h}33^{\rm m}40^{\rm s}$, $+30°46'0''$) to ($1^{\rm h}34^{\rm m}30^{\rm s}$, $+30°49'0''$) is prominent.

The surface mass density of molecular hydrogen was estimated by applying the ^{12}CO-to-H_2 conversion factor, $X_{\rm CO}=3\times10^{20}$ cm^{-2} (K km s^{-1})$^{-1}$ (Wilson & Scoville 1990) as follows:

$$\left(\frac{\Sigma_{\rm H_2}}{M_\odot\ {\rm pc}^{-2}}\right)=4.81\left(\frac{X_{\rm CO}}{3\times10^{20}\ {\rm cm}^{-2}\ ({\rm K\ km\,s}^{-1})^{-1}}\right)\times\left(\frac{I_{\rm CO}}{\rm K\ km\,s^{-1}}\right)\cos i, \quad (1)$$

where i is the inclination angle of galaxy ($i=51°$).

3.2. *Star formation rate*

We calculated the SFR according to the relation between the extinction-corrected Hα line emission and the SFR, as presented in Calzetti et al. (2007):

$$\begin{aligned}{\rm SFR}(M_\odot\ {\rm yr}^{-1})=5.3\times10^{-42}\,[&L(H\alpha)_{obs}\\&+(0.031\pm0.006)L(24\,\mu{\rm m})],\end{aligned} \quad (2)$$

in turn leading to

$$\Sigma_{\rm SFR}(M_\odot\,{\rm yr}^{-1}\,{\rm pc}^{-2}) = 5.0\times10^{-5}\,[\Sigma({\rm H}\alpha)_{\rm obs} + (0.031\pm0.006)\Sigma(24\,\mu{\rm m})]\cos i, \quad (3)$$

where the luminosities are in $\mathrm{erg\,s^{-1}}$ and L (24 μm) is expressed as $\nu\,L(\nu)$.

We use the Hα image of M33 as given by Hoopes & Walterbos (2000). It was obtained using the 0.6-m Burrell-Schmidt telescope at the Kitt Peak National Observatory. The dimensions of the CCD are 2048×2048 with a pixel size of $2''.03$ and the total field of view is approximately $70'\times70'$. The sensitivity is $0.8\times10^{-17}\,\mathrm{erg\,s^{-1}\,cm^{-2}\,arcsec^{-2}}$ (Hoopes et al. 2001).

We retrieved the 24-μm Multiband Imaging Photometer (MIPS: Rieke et al. 2004) datasets (AORs 3647744, 3648256, 3648512, 3648768) of the basic calibrated data (BCD) created by the Spitzer Science Center (SSC) pipeline from the Spitzer Space Telescope (Werner et al. 2004) data archive. The mosaics were assembled by gathering all the BCDs except first data frames of each observation because the first data frames have shorter integration times. The individual calibrated frames were processed using MOPEX (Makovoz & Khan 2005) for cosmic-ray rejection and background matching was applied to overlapping fields of view. The final dimension of the each mosaic was approximately $21'\times89'$. Then, we removed zodiacal light using the IRAF task "imsurfit." After removing the noisy pixels near the edges by trimming, the four images were aligned with their coordinates using an AIPS task "OHGEO" and combined using "COMB." The FWHM of PSF is $5''.7$.

The Hα and 24-μm images were convolved into the same angular resolution of the CO(J=1–0) data ($19''.3$) using the AIPS task "CONVL," regridded to $7''.5$ per pixel, and trimmed in order to match the CO (J=1–0) map using "OHGEO." The rms noise is $5\times10^{-7}\,\mathrm{erg\,s^{-1}\,cm^{-2}}$ in the Hα map, and $3\times10^{-5}\,\mathrm{erg\,s^{-1}\,cm^{-2}}$ in the 24-μm map. The resultant SFR image is shown in Fig. 2 with the overlaid CO (J=1–0) contours. The rms noises in the Hα and 24-μm maps result in a $\Sigma_{\rm SFR}$ error and a sensitivity limit of $5\times10^{-11}\,M_\odot\,\mathrm{yr^{-1}\,pc^{-2}}$.

Fig. 2 reveals a striking variety of star formation properties. In the regions where CO emission is detected, there is a large dispersion in the values of $\Sigma_{\rm SFR}$ of upto four orders of magnitude. For example, the most massive GMC at (α, δ) = ($1^{\rm h}33^{\rm m}9^{\rm s}.6$, $+30°49'7''.3$) has little star formation activity despite the large amount of molecular gas it contains. In the three major star-forming regions (NGC 604, NGC 595, and IC 133), there is a considerable difference of the amount in molecular gas associated with these star-forming regions is noticeable. NGC 604 has its associated GMCs at the same position, NGC 595 has the ones offset from it, and moreover, none of the GMCs are associated with IC 133.

4. DISCUSSION

Fig. 3 presents the relationship between the SFR and molecular hydrogen surface densities for four angular resolutions: $19''.3$ ($\sim$80 pc), $60''$ ($\sim$240 pc), $120''$ ($\sim$500 pc), $240''$ ($\sim$ 1 kpc). The data points with $\Sigma_{\rm H_2} < 2\sigma$ are omitted from each plot. The panel of $19''.3$ ($\sim$ 80 pc) resolution is the K-S law plot with the highest resolution for an extra-galaxy to date. Fig. 3 shows that apparent correlations exist between $\Sigma_{\rm H_2}$ and $\Sigma_{\rm SFR}$ at the resolution of $\sim$1 kpc, as already found in disk-averaged data of M33 (Heyer et al. 2004). The best least-squares fit for the $\sim$1 kpc resolution plot is

$$\log\Sigma_{\rm SFR} = (1.18\pm0.11)\log\Sigma_{\rm H_2} - (9.38\pm0.05). \quad (4)$$

Fig. 3 also shows that the correlation becomes looser with higher resolution, and it is hardly visible in the plot for $\sim$80 pc resolution. Although most of the $\Sigma_{\rm H_2}$ values are in the range of 10–40 $M_\odot\mathrm{pc^{-2}}$, $\Sigma_{\rm SFR}$ values exhibit a very wide range of approximately four orders of magnitude, from $\lesssim10^{-10}$ to $\sim10^{-6}M_\odot\mathrm{yr^{-1}pc^{-2}}$. This indicates that the K-S law becomes invalid at this resolution. That is, the K-S law is valid only for averaging SFR and gas mass in large scales of several hundred parsecs. Our resolution, $\sim$80 pc, has been smaller than such scale.

We can consider two possible causes of the breakdown of the K-S law at high spatial resolution. In grand design spiral galaxies, we often see an systematic offset between the molecular gas arms and the star forming arms as a result of the density wave and the time delay between the accumulation of gas and its ionization by newborn stars (e.g., Egusa et al. 2009). If such offset exists in M33, it may result in the breakdown of the K-S law when we observe the galaxy with a spatial resolution comparable to the offset. However, there is no such systematic offset between the CO and the star-forming (Hα and 24-μm) arm in M33, as shown in Fig. 2. Thus, the offset cannot be the cause of the breakdown of the K-S law in M33.

In the Milky Way, young clusters recede from their parent GMCs with velocities of at least $\sim$ 10 $\mathrm{km\,s^{-1}}$ (Leisawitz et al. 1989). As they evolve, the separation between them becomes unignorable and can be expected to be $\sim$ 100 pc at a cluster age of $\sim$ 10 Myr. This drift scale is comparable to our resolution $\sim$ 80 pc thus the separation could well lead to the scatter in our plot. However, the existence of HII regions without neighboring GMCs and GMCs without neighboring HII regions in M33, such as ones that we mentioned in the previous section, can not be explained by the drift only.

The second possible cause is the difference in evolutionary stages. As we have shown in Fig. 2, there is a large diversity in the star formation activity among GMCs. Some GMCs in the Milky Way are at least partially consumed and dissociated by newborn clusters (Leisawitz et al. 1989). GMCs of the same type are seen in Fig. 2 (i.e., one at (α, δ) = ($1^{\rm h}34^{\rm m}17^{\rm s}$, $30^{\rm d}52^{\rm m}00^{\rm s}$)). The diversity of star formation activity among GMCs arises from the evolutionary stages that each GMC goes through, as has been shown in NGC 604 (Miura et al. 2010). Kawamura et al. (2009) classified molecular clouds in the Large Magellanic Cloud into three types according to the activities of massive star formation: those with no signature of massive star formation, those with relatively small HII region(s), and those with both HII region(s) and young stellar cluster(s). They concluded that the difference among the GMCs indicates that there is a sequential connection between these three types. That is, molecular clouds are first formed; then, stars are formed in the molecular clouds; and finally, the newborn stars consume and dissociate the surrounding gas. This scenario is also applicable to M33,

as has already been shown in NGC 604 from comparison with warm/ dense gas traced by CO ($J=3$–2) emission lines (Tosaki et al. 2007).

Owing to our spatial resolution, which is comparable in scale to that of GMCs, we clearly have revealed the variety in the evolutionary stages among GMCs. The different evolutionary stages of GMCs are the main cause of the deviation from the K-S law. The higher the spatial resolution, the more individual star-forming regions and molecular clouds we can resolve, and the larger the deviations we see in the K-S law plots.

5. SUMMARY

We conducted on-the-fly mapping observations of the northern part of M33 ($30' \times 20'$) in ^{12}CO ($J=1$–0) emission lines with the 45-m telescope at the Nobeyama Radio Observatory (NRO). We tested the relationship between the molecular gas mass and the SFR in an external galaxy with the highest resolution ($\sim$80 pc) to date. We found that the star-forming activities in the GMC scale exhibit a wide range of up to four orders-of-magnitude, such that $\Sigma_{\rm SFR} \lesssim 10^{-10}$ to $\sim 10^{-6} M_\odot {\rm yr}^{-1}$ pc^{-2}, whereas their $\Sigma_{\rm H_2}$ values are mostly confined in the range of 10–40 $M_\odot$ pc^{-2}. We also found that the K-S law of H_2 gas, $\Sigma_{\rm SFR} \propto \Sigma_{\rm H_2}^n$ becomes invalid at the scale of GMCs ($\sim$80 pc). The breakdown of the K-S law is attributed to the fact that the drift of newborn clusters from their parent GMCs and the difference in the evolutionary stages of GMCs become apparent at this spatial resolution.

We would like to thank Rene Walterbos for kindly providing us with the Hα image of M33. S. O. was financially supported by the Global COE Program "The Physical Sciences Frontier", MEXT, Japan. Nobeyama Radio Observatory is a branch of the National Astronomical Observatory of Japan, National Institutes of Natural Sciences.

REFERENCES

Calzetti, D., et al. 2007, ApJ, 666, 870
Egusa, F., Kohno, K., Sofue, Y., Nakanishi, H., & Komugi, S. 2009, ApJ, 697, 1870
Engargiola, G., Plambeck, R. L., Rosolowsky, E., & Blitz, L. 2003, ApJS, 149, 343
Freedman, W. L., Wilson, C. D., & Madore, B. F. 1991, ApJ, 372, 455
Heyer, M. H., Corbelli, E., Schneider, S. E., & Young, J. S. 2004, ApJ, 602, 723
Hoopes, C. G., & Walterbos, R. A. M. 2000, ApJ, 541, 597
Hoopes, C. G., Walterbos, R. A. M., & Bothun, G. D. 2001, ApJ, 559, 878
Kawamura, A., et al. 2009, ApJS, 184, 1
Kennicutt, R. C., Jr. 1998, ApJ, 498, 541
Kennicutt, R. C., Jr., et al. 2007, ApJ, 671, 333
Komugi, S., Sofue, Y., Nakanishi, H., Onodera, S., & Egusa, F. 2005, PASJ, 57, 733
Leisawitz, D., Bash, F. N., & Thaddeus, P. 1989, ApJS, 70, 731
Makovoz, D., & Khan, I. 2005, in ASP Conf. Ser. 347, Astronomical Data Analysis Software and Systems XIV, P. Shopbell, M. Britton, & R. Ebert, 81
Miura, R., et al. 2010, ApJ, submitted.
Rieke, G. H., et al. 2004, ApJS, 154, 25
Rosolowsky, E., Keto, E., Matsushita, S., & Willner, S. P. 2007, ApJ, 661, 830
Sawada, T., et al. 2008, PASJ, 60, 445
Schmidt, M. 1959, ApJ, 129, 243
Sunada, K., Yamaguchi, C., Nakai, N., Sorai, K., Okumura, S. K., & Ukita, N. 2000, in CPIE Conf. Ser. ed. H. R. Butcher, 4015, 237
Tosaki, T., Miura, R., Sawada, T., Kuno, N., Nakanishi, K., Kohno, K., Okumura, S. K., & Kawabe, R. 2007, ApJ, 664, L27
Verley, S., Corbelli, E., Giovanardi, C., & Hunt, L. K. 2010, A&A, 510, A64
Werner, M. W., et al. 2004, ApJS, 154, 1
Wilson, C. D., & Scoville, N. 1989, ApJ, 347, 743
Wilson, C. D., & Scoville, N. 1990, ApJ, 363, 435
Wong, T., & Blitz, L. 2002, ApJ, 569, 157

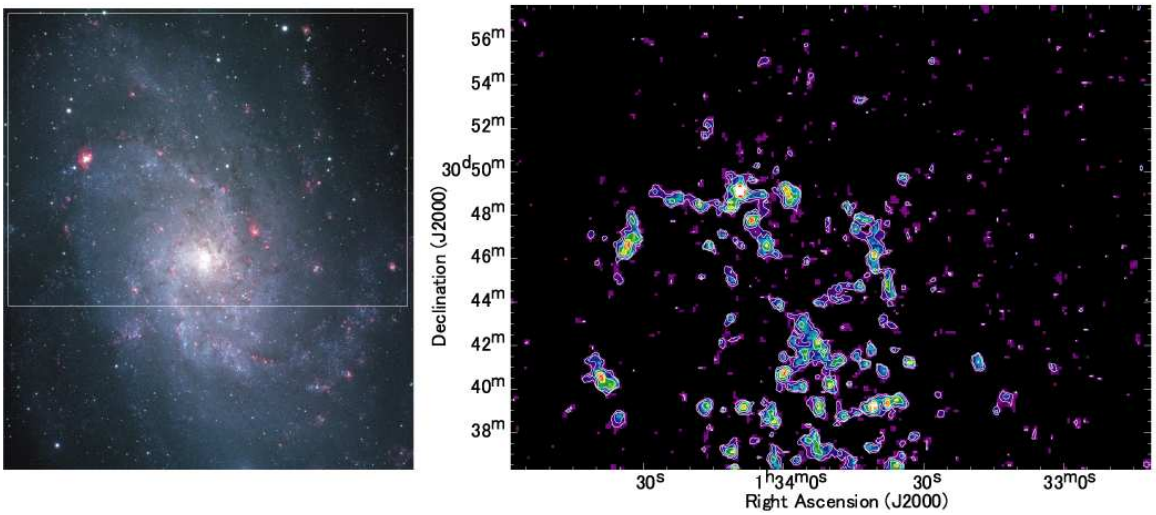

FIG. 1.— (Left) BVHα image of M33 taken with SUBARU Suprime-Cam ($30' \times 20'$): courtesy of V. Vansevicius, S. Okamoto, and N. Arimoto. The rectangle represents our mapping area of CO ($J = 1$–0) ($30' \times 20'$). (Right) Zeroth moment map (smoothed and clipped integrated intensity map) of the CO ($J = 1$–0) emission lines. The contour levels are 1, 2, 4, 6, and 8 K km s^{-1}, respectively.

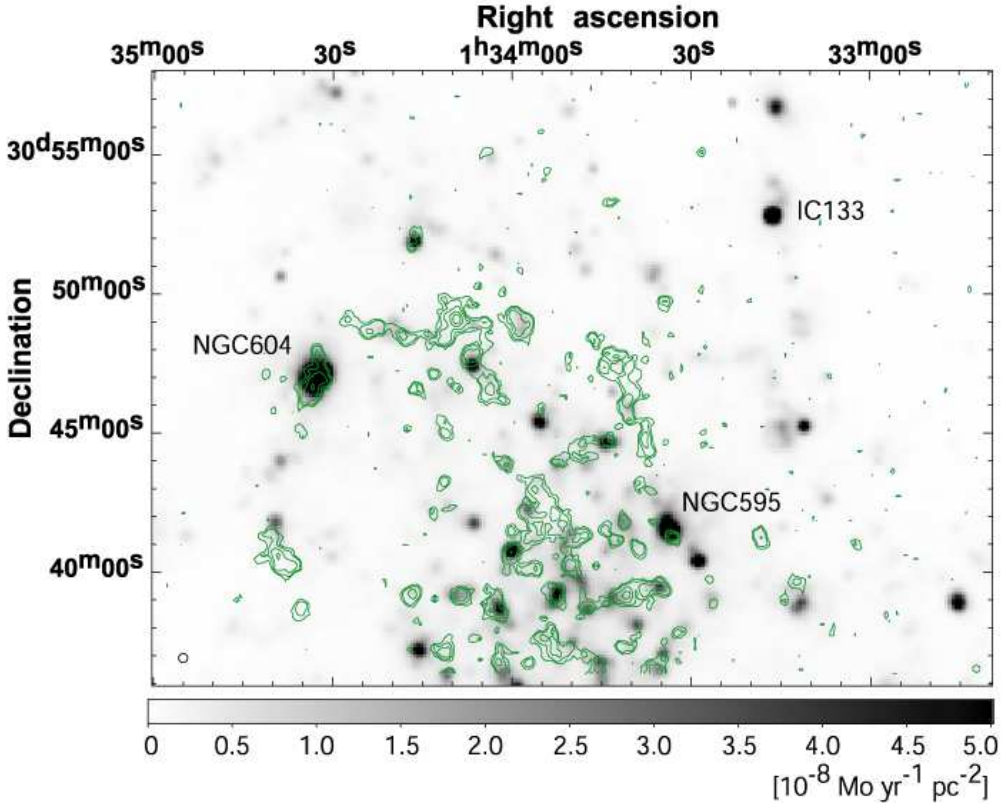

FIG. 2.— CO integrated intensity map (contour) overlaid on the SFR map convolved into $19''.3$ resolution. The contour levels are 1, 2, 4, 8, and 16 K km s^{-1}. The circle at the left bottom represents the beam size.

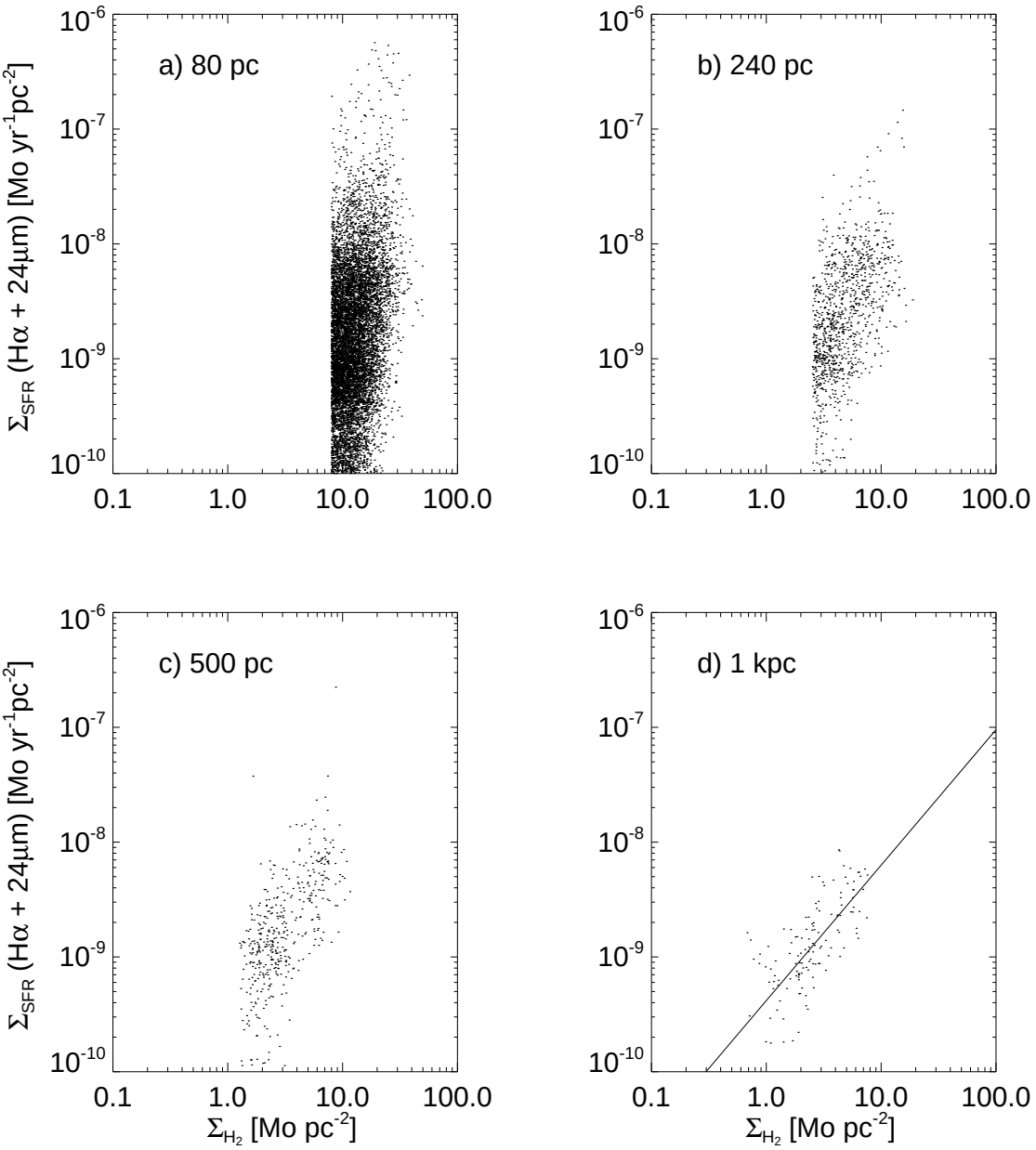

FIG. 3.— Star formation rate per unit area ($\Sigma_{\rm SFR}$) versus surface density of H_2 gas ($\Sigma_{\rm H_2}$) for four different resolutions: (a) 19″.3 ($\sim$ 80 pc), (b) 60″ ($\sim$ 240 pc), (c) 120″ ($\sim$ 500 pc), and (d) 240″ ($\sim$ 1 kpc), respectively. The data points with $\Sigma_{\rm H_2} < 2\sigma$ were omitted from each panel. The line in the lower-right panel represents the best least-squares fit to the 240″ ($\sim$ 1 kpc) resolution data; $\log \Sigma_{\rm SFR} = (1.18 \pm 0.11) \log \Sigma_{\rm H_2} - (9.38 \pm 0.05)$.